3-D Source Seeking for Underactuated Vehicles Without Position Measurement

Jennie Cochran, *Member, IEEE*, Antranik Siranosian, *Student Member, IEEE*,
Nima Ghods, *Student Member, IEEE*, and Miroslav Krstic, *Fellow, IEEE*

***Abstract*—Our past work introduced source seeking methods for GPS-denied autonomous vehicles using only local signal measurement and operating in two dimensions. In this paper, we extend these results to three dimensions. The 3-D extensions introduce many interesting challenges, including the choice of vehicle models in 3-D, sensor placement to allow probing-based gradient estimation of an unknown signal field in 3-D, the question of what type of pattern of vehicle motion can be produced in an underactuated 3-D vehicle to allow tuning by single-loop or multiloop extremum seeking, and the shape of attractors, which become very complex in 3-D. We present two control schemes that address these questions. The first scheme focuses on vehicles with a constant forward velocity and the ability to actuate pitch and yaw velocities. The second scheme employs vehicles with constant forward and pitch velocities and actuate only the roll velocity. Our results include convergence analysis and simulation results.**

***Index Terms*—Adaptive control, localization, nonholonomic motion planning, underactuated robots.**

I. INTRODUCTION

A. Motivation

THE FIELD of study for autonomous vehicles operating without GPS or inertial navigation is an area of rapidly growing interest. In environments where GPS is unavailable and inertial navigation is too costly, such as urban, underground, and underwater environments, other methods must be employed to navigate vehicles. Extremum seeking applied to source seeking has been presented as a method for autonomous vehicles to locate a target that emits some sort of measurable signal [1]–[3]. This signal could be electromagnetic, acoustic, or the concentration of a chemical or biological agent. The extremum seeking method uses only the measurement of the signal from the vehicle's sensor, and then employs a periodic probing movement for the vehicle to navigate the field and locate the target. Results of applying this method to vehicles operating in two dimensions show its great potential for use in many applications [4].

B. Contribution

In this paper, we explore the use of extremum seeking for the navigation of vehicles operating in three dimensions, and present the first solution to the problem of localization and pursuit of signal sources using only local signal measurement and without position measurement in three dimensions. The extension of source seeking from two dimensions to three is interesting for several reasons, including the choice of vehicle models in 3-D, sensor placement to allow probing-based gradient estimation of an unknown signal field in 3-D, the question of what type of pattern of vehicle motion can be produced in an underactuated 3-D vehicle to allow tuning by single-loop or multiloop (one parameter or multiparameter) extremum seeking, and the shape of attractors that are challenging to characterize in 3-D. We choose a model that is easy to relate to several different types of vehicles and explore different types of actuation for these vehicles.

C. Literature

Other researchers have considered source seeking problems: Porat and Neohorai [5] looked at using vehicles modeled as point sources to track vapor emitting sources, Reddy *et al.* [6] explored pursuit and evasion trajectories, and Ogren *et al.* [7] and Klein *et al.* [8] looked at coordination of multiple vehicles for gradient climbing and target tracking, respectively. This paper is different in that the vehicle has no knowledge of its position or the position of the source, there is no communication between it and other entities, and it has nonholonomic dynamics. While we apply the extremum seeking methods to autonomous vehicles, many groups have used the extremum seeking method in their work outside of this field, including [9] in the soft landing of valve actuators, [10] and [11] in plasma current profiles for fusion reactors, [12] in nonlocal stability properties, [13] in adaptive flow control, [14] in separation control, [15] in active braking systems, [16] in thermoacoustic coolers, and [17] in human exercise machines.

D. Models and Control Schemes Designed

We present two control schemes for actuating an autonomous vehicle operating in three dimensions whose task is to locate a target that emits a signal that the vehicle can sense. The first scheme addresses vehicles that have a constant forward velocity and can actuate both yaw and pitch velocities. We refer to

---

Manuscript received February 11, 2008; revised July 10, 2008. First published January 21, 2009; current version published February 4, 2009. This paper was recommended for publication by Associate Editor A. Martinelli and Editor J.-P. Laumond upon evaluation of the reviewers' comments. This work was supported in part by the National Science Foundation (NSF), in part by the National Defense Science and Engineering Graduate (NDSEG) Fellowship, the Los Alamos National Laboratory, and in part by the Office of Naval Research (ONR) under Grant N00014-07-1-0741.

J. Cochran was with the Department of Mechanical and Aerospace Engineering, University of California, San Diego, CA 92093-0411 USA. She is now with ScienceOps, Bothell, WA 98011-8804 USA (e-mail: jcochran@ucsd.edu).

A. Siranosian and N. Ghods are with the Department of Mechanical and Aerospace Engineering, University of California, San Diego, CA 92093-0411 USA (e-mail: asiranosian@ucsd.edu; nimaghods@gmail.com).

M. Krstic is with the Department of Mechanical and Aerospace Engineering, University of California, San Diego, CA 92093-0411 USA, and also with the Cymer Center for Control Systems and Dynamics, University of California, San Diego, CA 92093-0403 USA (e-mail: krstic@ucsd.edu).

Color versions of one or more of the figures in this paper are available online at http://ieeexplore.ieee.org.

Digital Object Identifier 10.1109/TRO.2008.2008742

1552-3098/$25.00 © 2009 IEEE

this vehicle as the vehicle yaw and pitch actuated (VYPa). The second scheme addresses vehicles that also have a constant forward velocity, as well as a constant pitch velocity, but can only actuate the roll velocity. We refer to this vehicle as the vehicle roll actuated (VeRa).

E. *Organization of the Paper*

We start in Section II with an overview of the extremum seeking method applied to source seeking and then continue with Section III, in which the vehicle model is discussed. Sections IV and VII detail the VYPa and VeRa control schemes, respectively. Sections VI and VII present simulation results for each scheme. The nonlinearities in these systems give rise to interesting and complex behaviors. To analytically quantify some of these, Section V includes a local stability result and Section VII includes further analysis of the final trajectories seen in simulations of the VeRa scheme. We continue with Section VIII where we present the application of the method to level set tracing, a problem studied in [18]. Section IX concludes the paper with our intentions for future work.

II. OVERVIEW OF SOURCE SEEKING IN 2-D

Extremum seeking employs periodic forcing of a plant to perform nonmodel-based gradient estimation [19]. In its application to autonomous vehicles [1], the vehicles considered are kinematically constrained and have no position information available. It is assumed that a target creates some spatially distributed signal field whose shape is unknown, though its strength is known to be maximal at the target and decreasing away from it. Extremum seeking employs only a scalar measurement of the signal at the tip of the vehicle, periodic probing to search the vehicle's surroundings, and a demodulating signal that produces a bias input to turn the vehicle in the correct net direction. This combination has a built-in gradient estimation capability. One of the method's successes is simultaneously solving nonholonomic steering and adaptive optimization problems.

Our previous work was for vehicles in 2-D, modeled as the nonholonomic unicycle, $\dot{r}_c = ve^{j\theta}$, $\dot{\theta} = \Omega$, where r_c is the vector position of the vehicle center, θ is the vehicle orientation, and v and Ω are the forward and angular velocity inputs [3], [4]. These vehicles are given a constant forward velocity $v = V_c$, while the angular velocity is tuned by extremum seeking, $\Omega(t) = a\omega\cos(\omega t) + c\sin(\omega t)(s/s+h)[J(t)]$, where a, c, h, and ω are parameters of the control law, $(s/s+h)$ is the Laplace transform of a washout filter, and $J(t)$ is the signal reading from the vehicle sensor located at $r_s = r_c + Re^{j\theta}$. The first term $a\cos(\omega t)$ is a continuous periodic excitation of the angular velocity that allows the vehicle to probe the area and record differences in signal readings. The second term is a bias that turns the vehicle in the correct net direction and it is, in fact, an estimate of $\partial J(r_c, \theta)/\partial\theta$. The gain c is adjusted to make the vehicle's reaction to the signal field more or less aggressive. The result of applying this control law to the unicycle model is the exponential convergence of the vehicle to the vicinity of the signal source [1], as seen in Fig. 1.

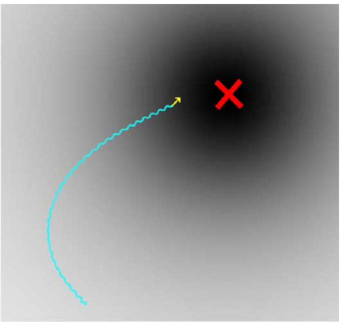

Fig. 1. 2-D vehicle employing extremum seeking to find a source.

III. VEHICLE MODEL

When extending the vehicle model from two dimensions to three, we must consider how to accurately represent a kinematically constrained vehicle that could support different vehicle configurations. We chose a kinematic model, depicted in Fig. 2(a). This figure shows a vehicle whose actuators, shown as cylinders with half arrows, can be used to impart surge, yaw, pitch, and roll velocities. The center of the vehicle is labeled r_c and the front of the vehicle is labeled r_f. The sensor, shown as a small sphere, is located above r_f at r_s. Fig. 2(b) contains a geometric interpretation of the drawing in Fig. 2(a). In the coordinate system shown, R_1 is the distance between the center r_c and the front r_f, while R_2 is the distance between the front r_f and the sensor r_s. The vector between r_f and r_s is always perpendicular to the vector between r_c and r_f. The pitch of the vehicle is defined by α, the azimuthal angle. The yaw of the vehicle is defined by θ, the polar angle. The third possible vehicle rotation, roll, is defined by ϕ and is measured in the plane containing $r_f QP$ relative to the plane containing $r_c AB$. The surge velocity V_c acts in the direction of $r_c r_f$, while the pitch velocity V_2 acts in the direction of $r_f r_s$. The angular rates $\dot{\alpha}$ and $\dot{\theta}$, or the angular rate $\dot{\phi}$, are available as control inputs.

The differential equation governing the center of the vehicle model depicted in Fig. 2 is

$$\dot{r}_c = V_c \begin{bmatrix} \cos(\alpha)\cos(\theta) \\ \cos(\alpha)\sin(\theta) \\ \sin(\alpha) \end{bmatrix} \tag{1}$$

where $r_c = (x_c, y_c, z_c)$. The sensor position is

$$r_s = r_c + R_1 \begin{bmatrix} \cos\alpha\cos\theta \\ \cos\alpha\sin\theta \\ \sin\alpha \end{bmatrix} + R_2 \begin{bmatrix} -\cos\phi\sin\alpha\cos\theta + \sin\phi\sin\theta \\ -\cos\phi\sin\alpha\sin\theta - \sin\phi\cos\theta \\ \cos\phi\cos\alpha \end{bmatrix} \tag{2}$$

where $r_s = (x_s, y_s, z_s)$.

This model is used for both control schemes presented. The similarities and differences will be summarized here and expanded in the next sections. In both schemes, the surge velocity V_c is set to a positive constant. In the first scheme, applied to the

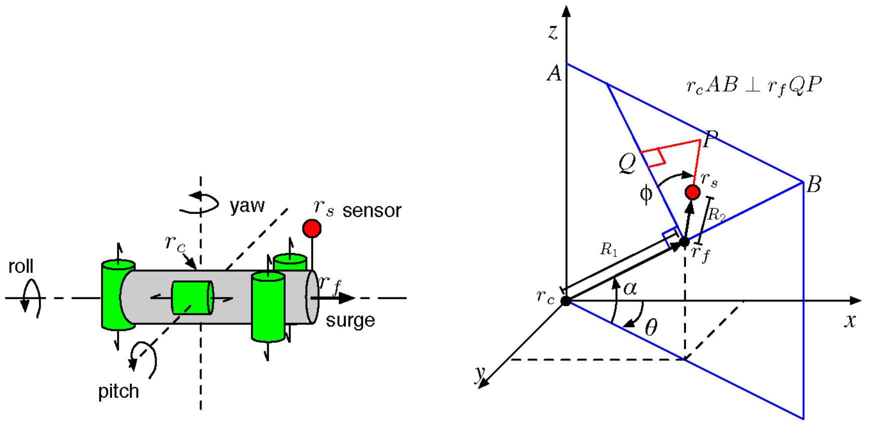

(a) (b)

Fig. 2. (a) Pictorial drawing of the 3-D vehicle. (b) Graphical interpretation of vehicle in 3-D.

VYPa, the sensor is placed at the tip of the vehicle, i.e., $R_2 = 0$, so the roll velocity and angle play no role. Extremum seeking is used to tune the two control inputs: the pitch and yaw velocities. In the second scheme, applied to the VeRA, the pitch velocity V_2 is also set to a nonzero constant and extremum seeking tunes only the roll velocity for control. The distance R_2 between the tip of the vehicle r_f and the sensor r_s must be nonzero in this case.

IV. VYPa Vehicles

The first scheme we address is for the VYPa. This vehicle has a constant forward velocity V_c, a constant roll angle of zero, and, as the name indicates, is equipped for actuation of its pitch and yaw velocities. The sensor is located at the tip of the vehicle, which equates to setting $R_2 = 0$ and results in $r_f = r_s$. Its position with respect to the vehicle center reduces to

$$r_s = r_c + R_1 \begin{bmatrix} \cos\alpha\cos\theta \\ \cos\alpha\sin\theta \\ \sin\alpha \end{bmatrix}. \tag{3}$$

As the surge velocity is constrained to one axis in the body frame and the angular velocity is always around an axis orthogonal to that of the surge velocity, this is the 3-D analog of the unicycle.

Fig. 3 shows a block diagram of the control applied to the VYPa, with extremum seeking used to tune the pitch and yaw velocities. When the roll angle is not actuated, tuning the pitch velocity is equivalent to tuning $\dot{\alpha}$ and tuning the yaw velocity is equivalent to tuning $\dot{\theta}$. The designer is free to choose the perturbation amplitudes a_α, a_θ, the perturbation frequencies ω_α, ω_θ, the extremum seeking gains c_α, $c_\theta, d_\alpha, d_\theta$, and the break frequency h of the filter. It should be noted that ω_θ can be the same as ω_α. The perturbation amplitudes a_α and a_θ can be increased to achieve better performance with flat gradients. The higher the perturbation frequencies, the more accurate the gradient estimation becomes, however, with a slower convergence rate. The VYPa model equations remain (1), while the control inputs, following from Fig. 3, are

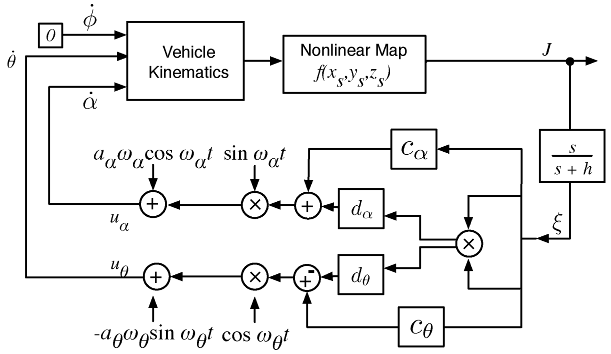

Fig. 3. Block diagram of extremum seeking (ES) control applied to the pitch and yaw velocities of the VYPa.

$$\dot{\alpha} = a_\alpha\omega_\alpha\cos(\omega_\alpha t) + \sin(\omega_\alpha t)\left(c_\alpha\xi + d_\alpha\xi^2\right) \tag{4}$$

$$\dot{\theta} = -a_\theta\omega_\theta\sin(\omega_\theta t) + \cos(\omega_\theta t)\left(c_\theta\xi - d_\theta\xi^2\right) \tag{5}$$

$$\dot{\phi} = 0 \tag{6}$$

where $(s/s+h)[J]$ is a washout filter applied to the sensor reading J.

As usual, the extremum seeking tuning consists of both: 1) periodic perturbations $a_\alpha\omega_\alpha\cos(\omega_\alpha t)$ and $-a_\theta\omega_\theta\sin(\omega_\theta t)$, which continuously probe the signal field and 2) bias terms $\sin(\omega_\alpha t)\left(c_\alpha\xi + d\xi^2\right)$ and $\cos(\omega_\theta t)\left(c_\theta\xi - d\xi^2\right)$, which turn the vehicle in the correct direction. The bias terms are composed of the sensor measurement that has been high-pass-filtered, demodulated, and multiplied by the appropriate gains.

V. Convergence of VYPa Vehicle

The dynamics of the closed loop are intricate. The complexity comes from the trigonometric nonlinearities in the vehicle model, the polynomial nonlinearity in the signal map, and the time-varying forcing applied by extremum seeking. The complexity of the system increases compared to the 2-D case as two extra states must be added to account for the dynamics in the extra dimension.

We assume that the nonlinear map defining the distribution of the signal field is quadratic and takes the form $J = f(r_s) = f^* - q_r|r_s - r^*|^2$, where r^* is the unknown maximizer, $f^* = f(r^*)$ is the unknown maximum, and q_r is an unknown positive constant. We define an output error variable $e = (h/s + h)[J] - f^*$, where $(h/s + h)[J]$ is a low-pass filter applied to the sensor reading J, which allows us to express ξ, the signal from the washout filter, as $\xi = (s/s + h)[J] = J - (s/s + h)[J] = J - f^* - e$. As a consequence, ξ and $\dot{e}$ take the following form

$$\xi = -(q_r|r_s - r^*|^2 + e) \tag{7}$$

$$\dot{e} = h\xi. \tag{8}$$

Before stating our main result, we introduce the set $\mathcal{T}_\delta$ defined by

$$\mathcal{T}_\delta = \left\{\rho - \delta \le \sqrt{(x_c - x^*)^2 + (y_c - y^*)^2} \le \rho + \delta\right\} \times \{|z_c - z^*| \le \delta\} \tag{9}$$

where

$$\rho = \sqrt{\frac{V_c J_0(\sqrt{2}a)}{\sqrt{2}c_\theta q_r R_1 J_1(\sqrt{2}a)}} \tag{10}$$

and point out that all of the parameters c_θ, c_α, d_θ, d_α, h, R_1, V_c, and q_r are positive, the parameters ω_α, and ω_θ are chosen such that $\omega_\alpha = \omega_\theta = \omega$, and $J_0(a)$ and $J_1(a)$ are Bessel functions of the first kind.

Theorem 1: Consider the system defined by (1), (3)–(5), (7), and (8) where the parameter a is chosen such that

$$4V_c\, J_0(\sqrt{2}a) > hR_1\left(4J_0(\sqrt{2}a) - \frac{(\sqrt{2}J_1(2a) + J_1(2\sqrt{2}a))}{J_1(\sqrt{2}a)}\right). \tag{11}$$

For sufficiently large ω, if $(x_c(0), y_c(0), z_c(0)) \in \mathcal{T}_\delta$ for sufficiently small $\delta > 0$, and if the quantities $|\alpha(0)|$, $|e(0) + q_r R_1^2 + [V_c J_0(\sqrt{2}a)/\sqrt{2}c_\theta R_1 J_1(\sqrt{2}a)]|$, and either $|\theta(0) - \arctan[(y_c - y^*)/(x_c - x^*)] + (\pi/2)|$ or $|\theta(0) - \arctan(y_c - y^*)/(x_c - x^*) - (\pi/2)|$, are all sufficiently small, then the trajectory of the vehicle center $r_c(t)$ exponentially converges to, and remains in the set $\mathcal{T}_{O(1/\omega)}$, and the sensor reading $J(t)$ converges exponentially to a periodic function of period $2\pi/\omega$ within $O(1/\omega)$ of

$$f^* - q_r R_1^2 - \frac{V_c J_0(\sqrt{2}a)}{\sqrt{2}c_\theta R_1 J_1(\sqrt{2}a)}. \tag{12}$$

Furthermore, the vehicle center locally exponentially converges to a solution of the form

$$x_c^{\mathrm{attr}_i}(t) = x^* + \tilde{r}_c^{\mathrm{attr}_i}(t)\cos(\theta^{*\mathrm{attr}_i}(t))\cos(\alpha^{*\mathrm{attr}_i}(t)) \tag{13}$$

$$y_c^{\mathrm{attr}_i}(t) = y^* + \tilde{r}_c^{\mathrm{attr}_i}(t)\sin(\theta^{*\mathrm{attr}_i}(t))\cos(\alpha^{*\mathrm{attr}_i}(t)) \tag{14}$$

$$z_c^{\mathrm{attr}_i}(t) = z^* + \tilde{r}_c^{\mathrm{attr}_i}(t)\sin(\alpha^{*\mathrm{attr}_i}(t)) \tag{15}$$

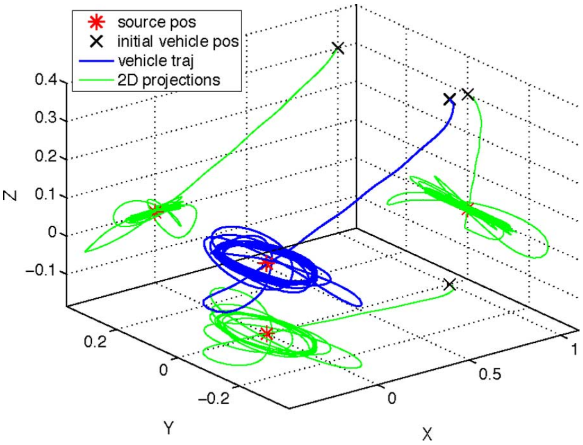

Fig. 4. Vehicle locating a static source that creates a signal field with spherical level sets. $V_c = 0.1, c_\theta = c_\alpha = 100, d_\theta = d_\alpha = 300, a = 0.5, \omega = 40, R_1 = 0.1, f^* = 1, q_r 1 =, h = 1.$

where $i \in \{0, 1\}$ and

$$\tilde{r}_c^{\mathrm{attr}_i}(t) = \left(\rho + \tilde{r}_\mu^{\mathrm{eq_i}} + \tilde{r}_{c_0}^{(2\pi/\omega)^{\mathrm{eq_i}}}(t)\right) \tag{16}$$

$$\theta^{*\mathrm{attr}_i}(t) = (-1)^i\left(\frac{V_c}{\rho}\left(1 + \lambda_\mu^{\mathrm{eq_i}}\right)t + \frac{V_c}{\rho}\beta_0^{(2\pi/\omega)^{\mathrm{eq_i}}}(t) + \gamma^{\mathrm{eq}_i}\right) \tag{17}$$

$$\alpha^{*\mathrm{attr}_i}(t) = \left(\alpha_\mu^{*\mathrm{eq_i}} + \alpha_0^{*(2\pi/\omega)^{\mathrm{eq_i}}}(t)\right) \tag{18}$$

and where $\tilde{r}_\mu^{\mathrm{eq}_i}$, $\alpha_\mu^{*\mathrm{eq}_i}$ are $O(1/\omega)$, $\tilde{r}_{c_0}^{(2\pi/\omega)^{\mathrm{eq}_i}}(t)$, $\alpha_0^{*(2\pi/\omega)^{\mathrm{eq}_i}}(t)$ are periodic with frequency ω, zero mean, and $O(1/\omega)$, $\lambda_\mu^{\mathrm{eq}_i}$ is $O(a^2) + O(1/\omega)$, $\beta_0^{(2\pi/\omega)^{\mathrm{eq}_i}}(t)$ is periodic with frequency ω, zero mean, and $O(a^2) + O(1/\omega)$, and γ^{eq_i} is a constant.

The 3-D attractor characterized in Theorem 1 is similar to the attractor seen in the 2-D unicycle with a constant forward velocity and tuned angular velocity. In the 2-D case, the vehicle converges to within an annulus in R^2 (of a particular radius and thickness) around the source. In the 3-D case, the vehicle converges to within the set $\mathcal{T}_{O(1/\omega)}$, which is inside a horizontal torus of thickness $O(1/\omega)$ with major radius ρ.

VI. ILLUSTRATION OF VYPA VEHICLE BEHAVIOR

The behavior exhibited by the vehicle is very interesting in terms of how it changes with the chosen parameters. We start this section by illustrating the behavior predicted by Theorem 1. We then examine scenarios that have parameter combinations that the theory does not address.

The following figures illustrate the behavior predicted in Theorem 1. Fig. 4 shows the vehicle converging to a "pseudoorbit" around a static source that produces a signal field with spherical level sets. Fig. 5 illustrates the different attractors seen when the parameter c is varied within the assumptions of Theorem 1. The radii of the attractors decrease as c increases, as predicted by the inverse dependence of ρ on c. Fig. 5 also shows the local residual behavior of the vehicle center that is averaged out in the proof. Fig. 6 illustrates that adding measurement noise to the simulation affects the performance, but does not change the result qualitatively. In highly noisy experiments,

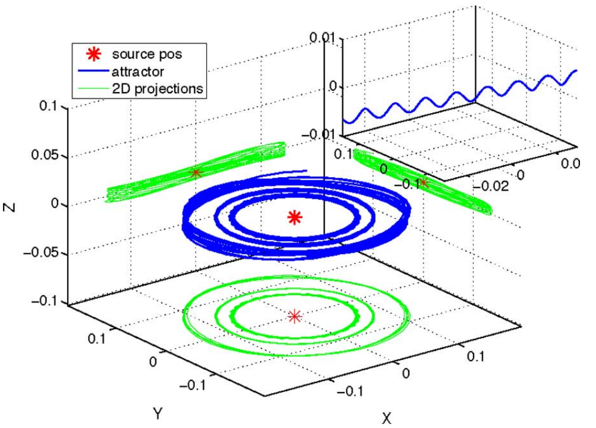

Fig. 5. Attractors resulting from different parameter configurations. The inset reveals the close-up behavior of the vehicle center. $V_c = 0.1, a = 0.5, \omega = 40, R_1 = 0.1, f^* = 1, q_r = 1, h = 1$. Outer attractor: $c_\theta = c_\alpha = 100, d_\theta = d_\alpha = 300$. Middle attractor: $c_\theta = 200, c_\alpha = 100, d_\theta = 600, d_\alpha = 300$. Inner attractor: $c_\theta = 300, c_\alpha = 100, d_\theta = 600, d_\alpha = 300$.

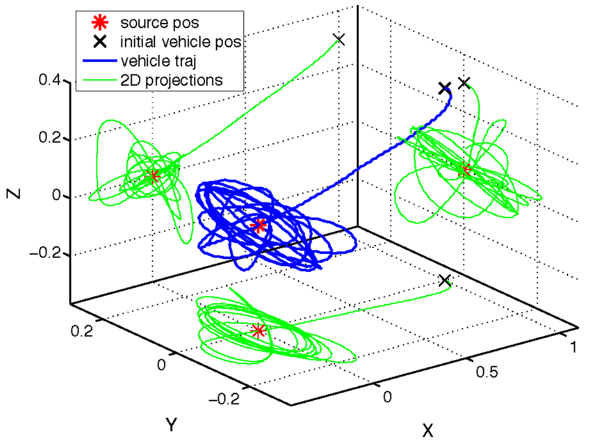

Fig. 6. Simulation from Fig. 4 with measurement noise ($\mu = 0, \sigma^2 = 0.5$) added to the simulation. $V_c = 0.1, c_\theta = c_\alpha = 100, d_\theta = d_\alpha = 300, a = 0.5, \omega = 40, R_1 = 0.1, f^* = 1, q_r = 1, h = 1$.

one would replace the washout filter by a bandpass filter, as was done in [20]. Fig. 7 shows the vehicle converging to an attractor around a static source that produces a signal field with ellipsoidal level sets. Though the theory presented here does not include ellipsoidal level sets, the convergence to an attractor in these cases is similar to the convergence seen in the 2-D cases where the target signal field is made up of elliptical level set [1]. The control law (4) and (5) also allows the vehicle to seek a moving source, as seen in Fig. 8, where the source follows a saddle pattern and produces spherical level sets that move with the source.

The proof of Theorem 1 relies on both d_α and d_θ being positive; however, convergent behavior is still seen when both are negative and when d_α is made negative. The fourth combination, when d_θ is negative and d_α is positive, results in unstable behavior. Fig. 9 illustrates the convergent behavior when both d_α and d_θ are negative. In this case, the attractor seen when both parameters are positive rotates and is twisted slightly. The attractor in this case is still similar to an "orbit." This differs from the third case, illustrated in Fig. 10, where the attractor is no

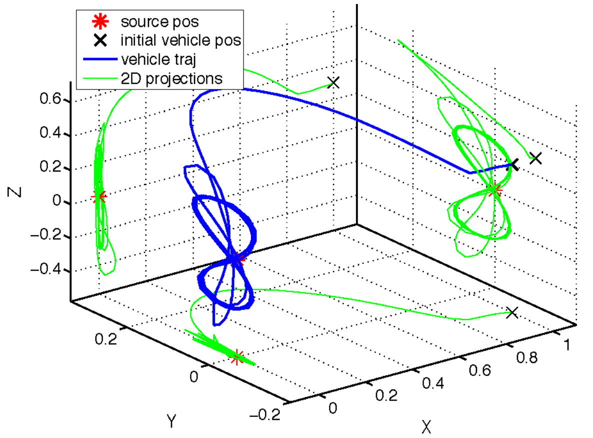

Fig. 7. Vehicle locating a target from a signal field with ellipsoidal level sets. The attractor seen has elements similar to the attractors seen in the 2-D case. $V_c = 0.1, c_\theta = c_\alpha = 100, d_\theta = 300, d_\alpha = 200, a = 0.5, \omega = 40, R_1 = 0.1, f^* = 1, q_x = 3, q_y = 2, q_z = 1, h = 1$.

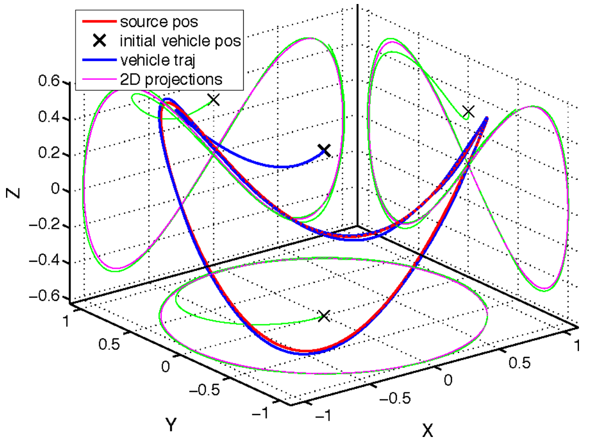

Fig. 8. Vehicle follows the moving source that creates a signal field with spherical level sets that move with the target. The target moves according to $(x_t(t), y_t(t), z_t(t)) = (\cos(0.05t), \sin(0.05t), 0.5\sin(0.1t)$. $V_c = 0.07, c_\theta = c_\alpha = 100, d_\theta = d_\alpha = 300, a = 0.5, \omega = 10, R_1 = 0.1$, $f^* = 1, q_r = 1, h = 1$.

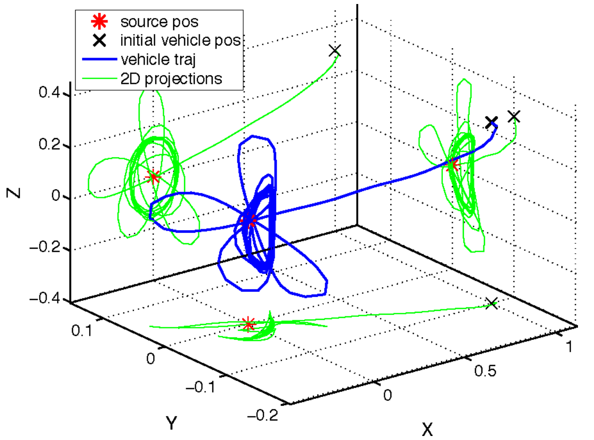

Fig. 9. Vehicle locates a source. Signal field has spherical level sets. The final attractor is rotated compared to other cases, but is still of an "orbit-like" form. $V_c = 0.1, c_\theta = c_\alpha = 100, d_\theta = 300, = d_\alpha = -300, a = 0.5, \omega = 40, R_1 = 0.1, f^* = 1, q_r = 1, h = 1$.

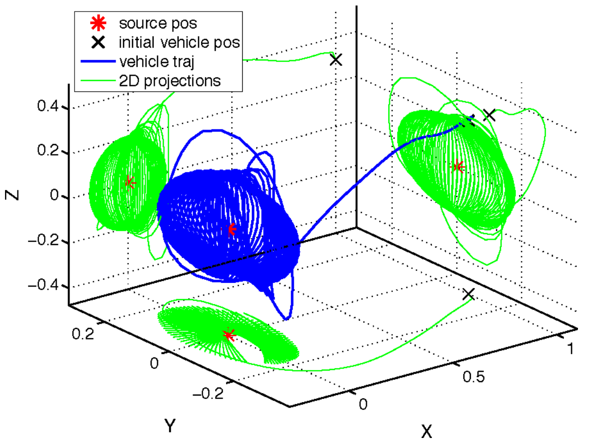

Fig. 10. Vehicle locates a source. Signal field has spherical level sets. The attractor is $O(1/\omega)$ within the surface of a sphere instead of an "orbit" type. $V_c = 0.2, c_\theta = c_\alpha = 100, d_\theta = 300, d_\alpha = -300, a = 0.5, R_1 = 0.1, \omega = 40, f^* = 1, q_r = 1, h = 1$.

longer of an "orbit" type. In this case, the vehicle moves around the surface of a sphere, staying within an $O(1/\omega)$ distance from the sphere.

VII. VERA VEHICLES

The second scheme presented is for the VeRa. We consider this vehicle configuration to show both the broad applicability of extremum seeking and its use for extremely underactuated vehicles. This vehicle has both a constant forward velocity V_c and a constant pitch velocity V_2. The only tunable input, as the name indicates, is the roll velocity. In this case, the sensor must be mounted off of the tip of the vehicle, which indicates $R_2 \neq 0$. When the pitch velocity V_2 is constant, the azimuthal and polar velocities become

$$\dot{\alpha} = \frac{V_2}{R_1}\cos\phi \tag{19}$$

$$\dot{\theta} = -\frac{V_2}{R_1}\frac{\sin\phi}{\cos\alpha}. \tag{20}$$

The VeRa model dynamics remain (1) with (19) and (20) governing the angles α and θ, and where u_ϕ is tuned by extremum seeking. The sensor coordinates also remain (2).

Fig. 11 shows a block diagram of the control applied to the VeRa, with extremum seeking used to tune the roll velocity according to the following algorithm:

$$\dot{\phi} = a\omega\cos(\omega t) + c\sin(\omega t)\frac{s}{s+h}[J]. \tag{21}$$

For a fuller understanding of the behavior displayed while employing the scheme (21), we look to averaging theory again.

Proposition 1: Over a finite time interval $[0, O(\omega)]$, the solutions of the system (1), (19)–(21) remain within $O(1/\omega)$ of the solutions of the following system:

$$\frac{d\tilde{r}_c^{\text{ave}}}{d\tau} = \frac{V_c}{\omega}(\cos(\alpha^{\text{ave}})\cos(\alpha^{*\text{ave}})\cos(\tilde{\theta}^{\text{ave}}) + \sin(\alpha^{\text{ave}})\sin(\alpha^{*\text{ave}})) \tag{22}$$

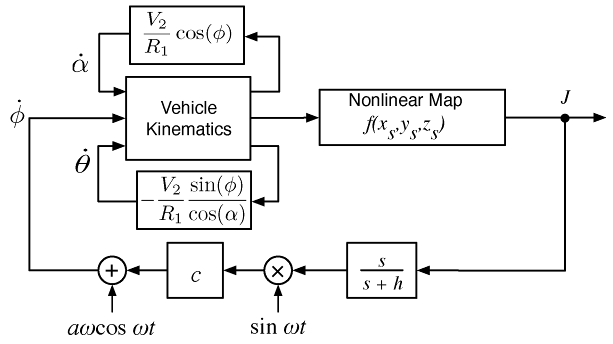

Fig. 11. Block diagram of ES control applied to the roll velocity of the VeRa.

$$\frac{d\alpha^{*\text{ave}}}{d\tau} = \frac{V_c}{\omega}\frac{1}{\tilde{r}_c^{\text{ave}}}(\sin(\alpha^{\text{ave}})\cos(\alpha^{*\text{ave}}) - \cos(\alpha^{\text{ave}})\sin(\alpha^{*\text{ave}})\cos(\tilde{\theta}^{\text{ave}})) \tag{23}$$

$$\frac{d\tilde{\theta}^{\text{ave}}}{d\tau} = \frac{-1}{\omega}\left(\frac{V_2 J_0(a)}{R_1}\frac{\sin(\hat{\phi}^{\text{ave}})}{\cos(\alpha^{\text{ave}})} + \frac{V_c}{\tilde{r}_c^{\text{ave}}}\frac{\cos(\alpha^{\text{ave}})}{\cos(\alpha^{*\text{ave}})}\sin(\tilde{\theta}^{\text{ave}})\right) \tag{24}$$

$$\frac{d\alpha^{\text{ave}}}{d\tau} = \frac{1}{\omega}\frac{V_2 J_0(a)}{R_1}\cos(\hat{\phi}^{\text{ave}}) \tag{25}$$

$$\begin{aligned}\frac{d\hat{\phi}^{\text{ave}}}{d\tau} = &-\frac{2cq_r R_2 J_1(a)\tilde{r}_c^{\text{ave}}}{\omega}\\ &\times(\cos(\alpha^{*\text{ave}})\cos(\hat{\phi}^{\text{ave}})\sin(\tilde{\theta}^{\text{ave}})\\ &-\sin(\hat{\phi}^{\text{ave}})(\sin(\alpha^{*\text{ave}})\cos(\alpha^{\text{ave}})\\ &-\cos(\alpha^{*\text{ave}})\sin(\alpha^{\text{ave}})\cos(\tilde{\theta}^{\text{ave}})))\end{aligned} \tag{26}$$

$$\begin{aligned}\frac{de^{\text{ave}}}{d\tau} = &-\frac{hq_r}{\omega}(\tilde{r}_c^{\text{ave}^2} + R_1^2 + R_2^2\\ &+2R_1\tilde{r}_c^{\text{ave}}(\cos(\alpha^{*\text{ave}})\cos(\alpha^{\text{ave}})\cos(\tilde{\theta}^{\text{ave}})\\ &+\sin(\alpha^{*\text{ave}})\sin(\alpha^{\text{ave}}))\\ &+2R_2 J_0(a)\tilde{r}_c^{\text{ave}}(\cos(\hat{\phi}^{\text{ave}})(\sin(\alpha^{*\text{ave}})\cos(\alpha^{\text{ave}})\\ &-\cos(\alpha^{*\text{ave}})\sin(\alpha^{\text{ave}})\cos(\tilde{\theta}^{\text{ave}}))\\ &+\cos(\alpha^{*\text{ave}})\sin(\hat{\phi}^{\text{ave}})\sin(\tilde{\theta}^{\text{ave}}))) - \frac{h}{\omega}e^{\text{ave}}\end{aligned} \tag{27}$$

where $\tilde{r}_c = \sqrt{(x_c - x^*)^2 + (y_c - y^*)^2 + (z_c - z^*)^2}$, $\alpha^* = \arctan(z_c - z^*/\sqrt{(x_c - x^*)^2 + (y_c - y^*)^2})$, $\theta^* = \arctan((y_c - y^*)/(x_c - x^*))$, $\tilde{\theta} = \theta - \theta^*$, and $\tau = \omega t$, $\hat{\phi} = \phi - a\sin(\omega t)$.

Proof: To prove this proposition, we start from the original error system

$$\dot{\tilde{r}}_c = V_c(\cos(\alpha)\cos(\alpha^*)\cos(\tilde{\theta}) + \sin(\alpha)\sin(\alpha^*))$$

$$\dot{\alpha}^* = \frac{V_c}{\tilde{r}_c}(\sin(\alpha)\cos(\alpha^*) - \cos(\alpha)\sin(\alpha^*)\cos(\tilde{\theta}))$$

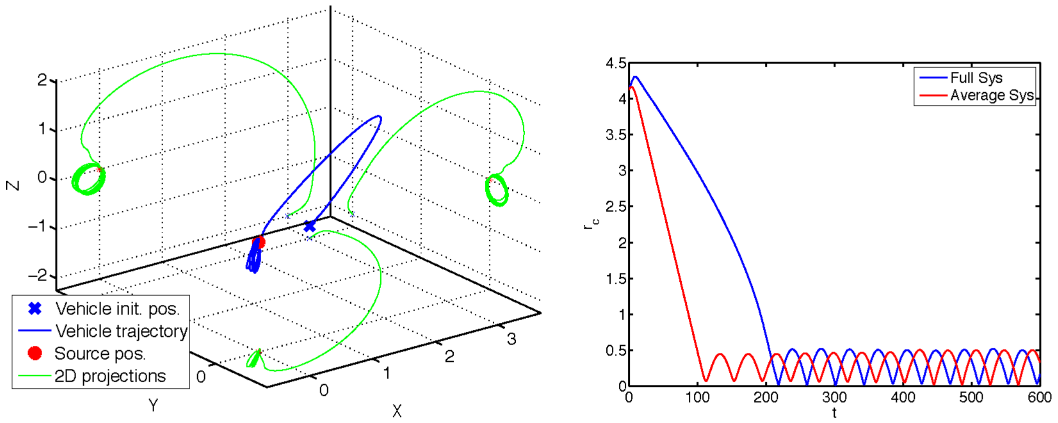

(a) (b)

Fig. 12. VeRa locates a static source. (a) Vehicle trajectory according to the full system equations is shown in a 3-D space, with 2-D projections shown on the grid walls. (b) Distance from the vehicle to the source is shown according to both the full system equations and the average system equations. $V_c = 0.04, V_2 = 0.02, c = 800, a = 1, \omega = 40, R_1 = 0.1, R_2 = 0.05, f^* = 1, q_r = 1, h = 1$.

$$
\begin{aligned}
\dot{\tilde{\theta}} &= -\left(\frac{V_2}{R_1}\frac{\sin(\phi)}{\cos(\alpha)} + \frac{V_c}{\tilde{r}_c}\frac{\cos(\alpha)}{\cos(\alpha^*)}\sin(\tilde{\theta})\right)\\
\dot{\alpha} &= \frac{V_2}{R_1}\cos(\phi)\\
\dot{\phi} &= a\omega\cos(\omega t) + c\sin(\omega t)\xi\\
\dot{e} &= h\xi\\
\xi &= -q_r\,(\tilde{r}_c^2 + R_1^2 + R_2^2\\
&\quad + 2R_1\tilde{r}_c(\cos(\alpha^*)\cos(\alpha)\cos(\tilde{\theta}) + \sin(\alpha^*)\sin(\alpha))\\
&\quad + 2R_2\tilde{r}_c(\cos(\alpha^*)\sin(\phi)\sin(\tilde{\theta})\\
&\quad + \cos(\phi)(\sin(\alpha^*)\cos(\alpha) - \cos(\alpha^*)\sin(\alpha)\cos(\tilde{\theta})))) - e
\end{aligned}
$$

and after shifting the variables by $\tau = \omega t$, $\hat{\phi} = \phi - a\sin(\omega t)$, and noting that the system equations are periodic in 2π, we find the average system (22)–(27). ■

We now use Proposition 1 to study approximately finite-time behavior of the system. The equilibria

$$
\begin{aligned}
&\left[r_c^{\mathrm{ave}^{\mathrm{eq}_i}}, \alpha^{*\mathrm{ave}^{\mathrm{eq}_i}}, \tilde{\theta}^{\mathrm{ave}^{\mathrm{eq}_i}}, \alpha^{\mathrm{ave}^{\mathrm{eq}_i}}, \hat{\phi}^{\mathrm{ave}^{\mathrm{eq}_i}}, e^{\mathrm{ave}^{\mathrm{eq}_i}}\right]\\
&= \left[\frac{V_c R_1}{V_2 J_0(a)}, 0, (-1)^i\frac{\pi}{2}, 0, (-1)^{(i+1)}\frac{\pi}{2},\right.\\
&\quad \left. - q_r\left(\frac{V_c^2 R_1^2}{V_2^2 J_0(a)^2} + R_1^2 + R_2^2 - 2R_2\frac{V_c R_1}{V_2 J_0(a)}\right)\right] \qquad (28)
\end{aligned}
$$

where $i \in \{0, 1\}$ have a characteristic polynomial given by

$$
\begin{aligned}
&\left((\omega s)^2 + \frac{V_2^2 J_0(a)^2}{R_1^2}\right)(\omega s + h)\\
&\quad \times\left((\omega s)^3 + \frac{cV_c R_1}{V_2 J_0(a)}(\omega s)^2 + c\frac{V_c V_2 J_0(a)}{R_1}\right) = 0. \qquad (29)
\end{aligned}
$$

As these equilibria are unstable, averaging theory does not yield a full characterization of the system attractors. However, this does not necessarily rule out a more complex attractor. We note that the following form of exact solutions to the average system (22)–(27):

$$
\tilde{\theta}^{\mathrm{ave}}(t) = m\pi \qquad (30)
$$

$$
\hat{\phi}^{\mathrm{ave}}(t) = n\pi \qquad (31)
$$

$$
\alpha^{\mathrm{ave}}(t) = (-1)^n\frac{V_2 J_0(a)}{R_1}t + c_1 \qquad (32)
$$

$$
\tilde{r}_c^{\mathrm{ave}}(t) = \sqrt{\begin{array}{c}\left((-1)^{n+1}\frac{V_c R_1}{V_2 J_0(a)}\cos(\alpha^{\mathrm{ave}}(t)) + c_2\right)^2\\ + \left((-1)^{n+m}\frac{V_c R_1}{V_2 J_0(a)}\sin(\alpha^{\mathrm{ave}}(t)) + c_3\right)^2\end{array}} \qquad (33)
$$

$$
\alpha^{*\mathrm{ave}}(t) = \arctan\left(\frac{(-1)^{n+1}(V_c R_1/V_2 J_0(a))\cos(\alpha^{\mathrm{ave}}(t)) + c_2}{(-1)^{n+m}(V_c R_1/V_2 J_0(a))\sin(\alpha^{\mathrm{ave}}(t)) + c_3}\right) \qquad (34)
$$

$$
e^{\mathrm{ave}}(t) = \mathrm{e}^{-ht}\left(\int_0^t f(\hat{t})\mathrm{e}^{h\hat{t}}\,d\hat{t} + c_4\right) \qquad (35)
$$

$$
\begin{aligned}
f(\hat{t}) = -hq_r\Bigg(&\tilde{r}_c^{\mathrm{ave}}(\hat{t})^2 + R_1^2 + R_2^2 + 2R_1((-1)^m c_3\\
&\times\cos(\alpha^{\mathrm{ave}}(\hat{t})) + c_2\sin(\alpha^{\mathrm{ave}}(\hat{t})))\\
&+ 2R_2 J_0(a)(-1)^n\Bigg(c_2\cos(\alpha^{\mathrm{ave}}(\hat{t})) + (-1)^{m+1}c_3\\
&\times\sin(\alpha^{\mathrm{ave}}(\hat{t})) - \frac{V_c R_1}{V_2 J_0(a)}\Bigg)\Bigg) \qquad (36)
\end{aligned}
$$

where n, and m are integers and c_1, c_2, c_3, and c_4 are constants, are very close to solutions observed by simulation of the full system. Fig. 12 shows the trajectory of the vehicle according to the full system equations as well as the trajectory of $\tilde{r}_c$ according to both the full system and average system equations.

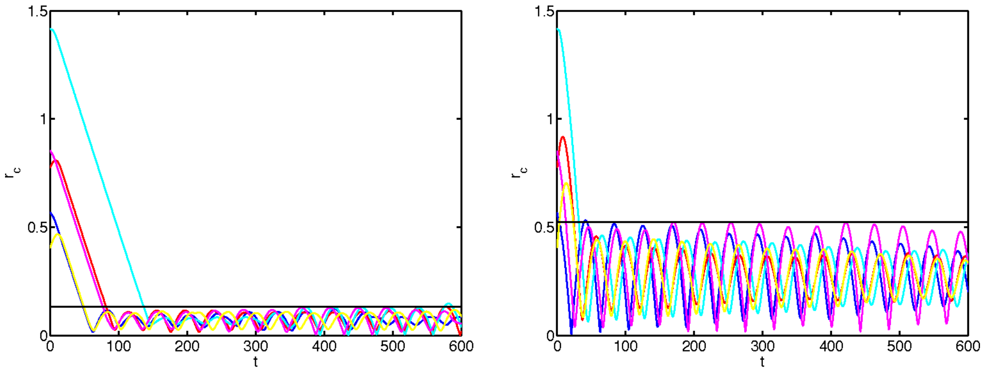

(a) (b)

Fig. 13. VeRa distance to source. (a) and (b) Vehicle locating a static source. The different lines indicated different initial conditions. The runs appear to be bounded by the quantity: $2V_1R_1/V_2J_0(a)$, which is shown as the black line above the distance oscillations, enforcing the observation that the ratio of $V_c : V_2$ determines tight or wide turns. For all runs, $c = 800, a = 1, \omega = 40, R_1 = 0.1, R_2 = 0.05, f^* = 1, q_r = 1, h = 1$. (a) $V_c = 0.01, V_2 = 0.02$. (b) $V_c = 0.04, V_2 = 0.02$.

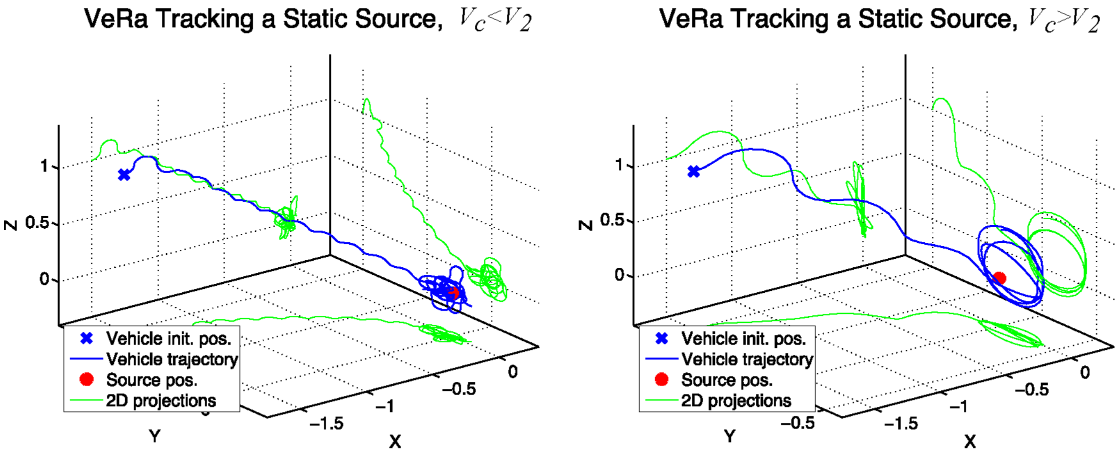
VeRa Tracking a Static Source, $V_c < V_2$

VeRa Tracking a Static Source, $V_c > V_2$

(a) (b)

Fig. 14. VeRa tracking a static source. For both runs, $c = 400, a = 1, \omega = 30, R_1 = 0.1, R_2 = 0.05, f^* = 1, q_x = 1, q_y = 0.5, q_z = 0.75, h = 1$. (a) Tight curly trajectory of the vehicle center is a result of $V_c < V_2$. $V_c = 0.028, V_2 = 0.055$. (b) Wide turns of the vehicle center trajectory are a result of $V_c > V_2$. $V_c = 0.04, V_2 = 0.02$.

The solution (30)–(36) defines a single repeating “loop” with radius $V_cR_1/V_2J_0(a)$ and unknown center. The drifting of these loops that is seen in the full simulation is presumably due to the system dynamics that are averaged out, similar to the drifting in the VYPa and 2-D solutions that lead to the attractors not being periodic. The frequency of r_c^2 is predicted by the known parameters $V_2J_0(a)/R_1$, while the point that the solution for $\tilde{r}_c^2$ oscillates about $(V_cR_1/V_2J_0(a))^2 + c_2^2 + c_3^2$, and the amplitude of these oscillations $2(V_cR_1/V_2J_0(a))\sqrt{c_2^2 + c_3^2}$ depend on unknown constants c_2, c_3. This leads to the question, is a bound on c_2, c_3, and thus, the trajectories, seen in simulations? Fig. 13 shows the path $\tilde{r}_c$ takes given different initial conditions. Each trajectory appears to be bounded by $2V_cR_1/V_2J_0(a)$. This explanation is enforced by the observation that when $V_c < V_2$, the vehicle trajectory is tight and curly, whereas when $V_c > V_2$, the trajectory consists of wide turns, as seen in Figs. 14 and 15.

Though in the case of a VYPa vehicle, the addition of a d term to the control law changes the qualitative behavior of the system (from having marginally stable attractor to having an exponentially stable attractor), the addition of a d term to the VeRa vehicle control law

$$\dot{\phi} = a\omega\cos(\omega t) + \sin(\omega t)(c\xi - d\xi^2)$$

$$\xi = \frac{s}{s+h}[J]$$

does not have the same effect. The effect of this additional term is seen only in the transient and is readily seen when $V_c \ll V_2$. Fig. 16 highlights the difference. Without a d term, the point in the middle of the vehicle, r_f, makes an unusual but consistent quadruple figure eight pattern, while the vehicle is on its way to the source. With the d term, the pattern shrinks to a single figure eight pattern. However, once the vehicle finds the source and starts moving around it, the vehicle enters a fundamentally different motion and the d term has no useful effect.

VIII. OTHER APPLICATIONS

The use of extremum seeking for navigation of vehicles in three dimensions extends beyond source seeking. This method

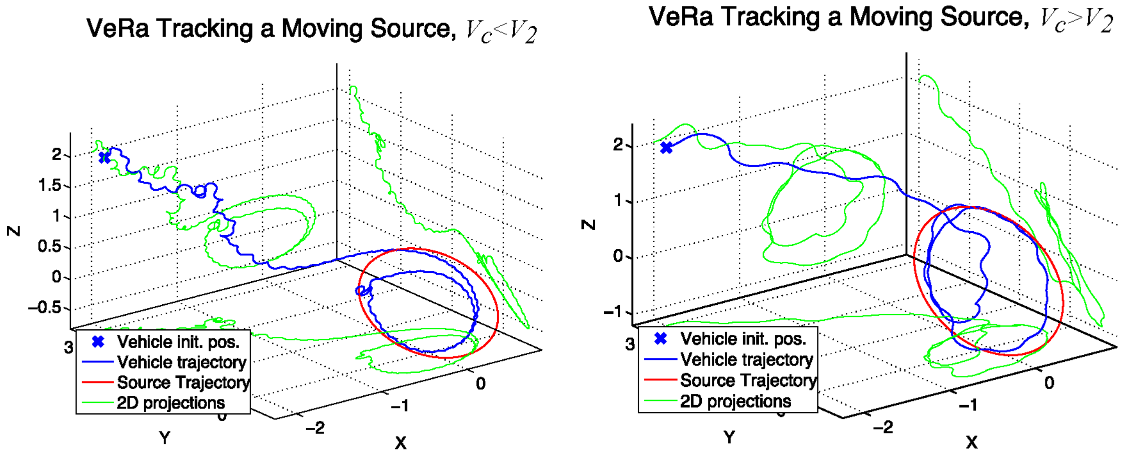

(a) (b)

Fig. 15. Trajectory of the center of a VeRa vehicle tracking a moving source. The source moves according to $(x_t(t), y_t(t), z_t(t)) = (a_t \cos(\omega_t t), a_t \sin(\omega_t t), a_{tz} \sin(\omega_{tz} t))$. For both runs, $c = 400, a = 1, \omega = 30, R_1 = 0.1, R_2 = 0.05, f^* = 1, q_x = 1, q_y = 0.5, q_z = 0.75, h = 1$. (a) $V_c = 0.028, V_2 = 0.055, a_t = 0.7, a_{tz} = 0.6, \omega_t = 0.035, \omega_{tz} = 0.035$. (b) $V_c = 0.04, V_2 = 0.02, a_t = 0.75, a_{tz} = 1, \omega_t = 0.0385, \omega_{tz} = 0.0385$.

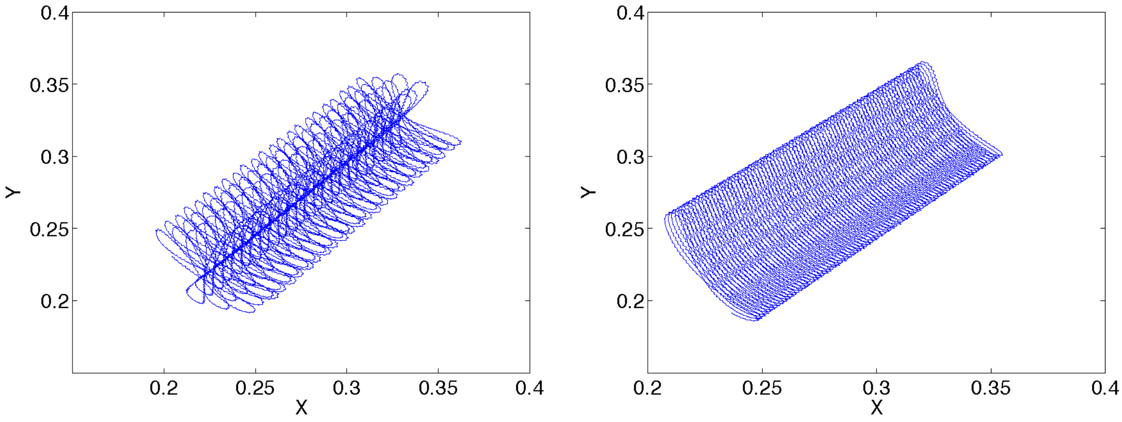

(a) (b)

Fig. 16. Motion of vehicle front r_f during transitive journey toward the source. The addition of the d term to the control law changes the pattern r_f makes as it moves. (a) $d = 0$. (b) $d = 1200$. The other system parameters are $V_c = 0.002, V_2 = 0.02, c = 400, a = 1, \omega = 30, R_1 = 0.1, R_2 = 0.05, f^* = 1, q_x = 1, q_y = 0.5, q_z = 0.75, h = 1$.

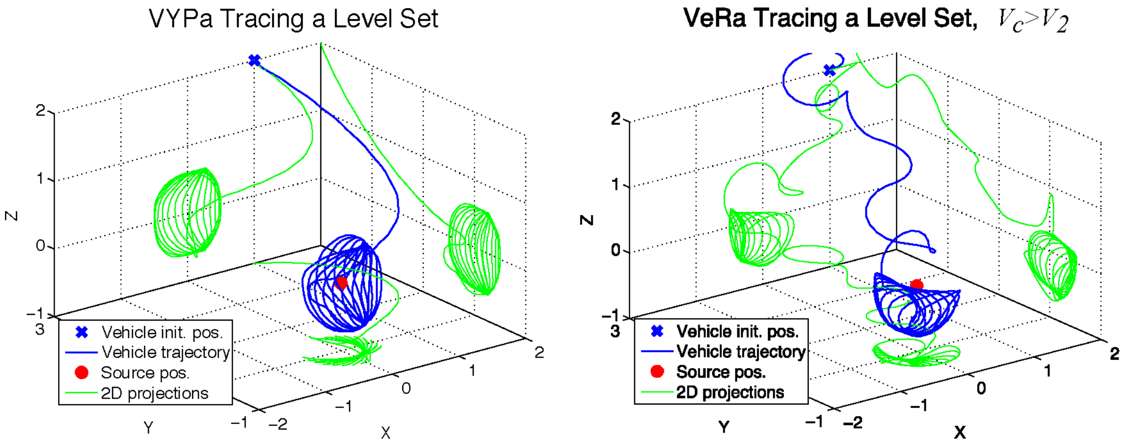

(a) (b)

Fig. 17. Trajectories of the center of vehicles tracing level sets are shown. For both runs, $f^* = 1, q_x = 1, q_y = 1, q_z = 0.5, J_d = 0.8$. (a) VYPa tracing a level set. $V_1 = 0.11, c = 50, a = 0.5, \omega = 10, R_1 = 0.1, h = 1$. (b) VeRa tracing a level set. $V_c = 0.07, V_2 = 0.02, c = 500, a = 0.75, \omega = 10, R_1 = 0.1, R_2 = 0.05, h = 1$.

can also be used to explore the domain of the signal field. Other groups have looked at isoline/boundary/level set tracing [21]. However, these methods require either multiple agents that must communicate, or require multiple sensors on a single agent. A potential difference (PD) control strategy for level set tracing without position measurement in 2-D was analyzed in [18].

By employing a simple modification to the extremum seeking tuning, both the VYPa and VeRa can find and trace 3-D level sets with only one sensor and without communication with other entities. This modification changes the input to the control laws from the sensor reading J to the quantity $-|J - J_d|$, where J_d is the desired level set value. The absolute value operator is used to retain the shape of the original signal field, as opposed to another operator, such as the square of the difference. The control law in each case then becomes $u_k(t) = a_k \omega_k \cos(\omega_k t) + c_k \sin(\omega_k t)(s/s + h)\,[-|J(t) - J_d|]$ for $k \in \{\theta, \alpha, \phi\}$. Fig. 17(a) and (b) shows the differences in how the VYPa and VeRa trace out the same level set on the same signal field. Note that the vehicles naturally move around the entire 3-D space instead of repeatedly tracing out the same curve within the level set.

IX. CONCLUSION

We have shown how the extremum seeking method can be extended to vehicles with various actuating capabilities operating in three dimensions for carrying out tasks, such as source seeking and level set tracing. The stability results presented, which are local, extend the 2-D work done previously, highlight the areas in which the 3-D schemes are more complex, and introduce new challenges in analysis.

In case of the VeRa design, it seems very hard to prove stability of an attractor for the motion of the vehicle near the source, though the simulation evidence is overwhelming regarding the existence of such an attractor, which is very complex, as the vehicle performs “loop” motions near the source with varying azimuthal and polar orientations and varying positions of the center of the loop relative to the position of the source. The reason for this complexity, compared to the VYPa system, is that only a single input (roll rate) is used to pursue source seeking with the six-state kinematic VeRA system. While the value of the averaging method is in simultaneously determining the existence of a periodic solution for a (part of, or an entire) system, for the VeRa system, it seems that the existence of an attractor would require one to find an analytical periodic solution of the entire nonlinear time-varying system (1), (2), (19)–(21) *before* applying averaging.

The designs in this paper are suitable for the underwater environment, where position and attitude information is difficult to obtain, especially over longer periods of time. The method in this paper enables the vehicle to converge to a point/area in space where a signal (chemical, thermal, electromagnetic, and acoustic) is the highest. Adding a communication element, such as relaying the location information back to a base station, is a separate question, as it requires position awareness. The methods in this paper are particularly compelling for applications where the primary objective is guiding a vehicle to a source.

While a two-layer approach employing position awareness, where path planning is decoupled from trajectory tracking, might outperform the designs in this paper, the simplicity (and effectiveness) of the approach makes it suitable as a candidate strategy for large fleets of simple, small autonomous underwater vehicles.

In the future, we plan to explore 3-D boundary/level set tracing for processes governed by diffusion and/or convection.

APPENDIX

Proof of Theorem 1: We start the proof by defining the shifted variables

$$\hat{r}_c = r_c - r^* \tag{37}$$

$$\hat{\alpha} = \alpha - a\sin(\omega t) \tag{38}$$

$$\hat{\theta} = \theta - a\cos(\omega t) \tag{39}$$

$$\tau = \omega t \tag{40}$$

and noting their dynamics

$$\frac{d\hat{r}_c}{d\tau} = \frac{V_c}{\omega}\begin{bmatrix}\cos(\hat{\alpha} + a\sin(\tau))\cos(\hat{\theta} + a\cos(\tau))\\ \cos(\hat{\alpha} + a\sin(\tau))\sin(\hat{\theta} + a\cos(\tau))\\ \sin(\hat{\alpha} + a\sin(\tau))\end{bmatrix} \tag{41}$$

$$\frac{d\hat{\alpha}}{d\tau} = \frac{1}{\omega}(c_\alpha \xi \sin(\tau) + d_\alpha \xi^2 \sin(\tau)) \tag{42}$$

$$\frac{d\hat{\theta}}{d\tau} = \frac{1}{\omega}(c_\theta \xi \cos(\tau) - d_\theta \xi^2 \cos(\tau)). \tag{43}$$

We now redefine r_c by its spherical coordinates

$$\tilde{r}_c = |\hat{r}_c| = \sqrt{\hat{x}_c^2 + \hat{y}_c^2 + \hat{z}_c^2} \tag{44}$$

$$\hat{r}_c = \tilde{r}_c \begin{bmatrix}\cos(\alpha^*)\cos(\theta^*)\\ \cos(\alpha^*)\sin(\theta^*)\\ \sin(\alpha^*)\end{bmatrix} \tag{45}$$

$$\tan(\theta^*) = \frac{\hat{y}_c}{\hat{x}_c} \tag{46}$$

$$\tan(\alpha^*) = \frac{\hat{z}_c}{\sqrt{\hat{y}_c^2 + \hat{x}_c^2}}. \tag{47}$$

Using these new definitions, the expression for ξ is

$$\xi = -q_r(\tilde{r}_c^2 + R_1^2 + 2\tilde{r}_c R_1 \xi_c) - e \tag{48}$$

$$\begin{aligned}\xi_c = {} & \cos(\hat{\alpha} + a\sin(\tau))\cos(\alpha^*)\cos(\hat{\theta} - \theta^* + a\cos(\tau))\\ & + \sin(\hat{\alpha} + a\sin(\tau))\sin(\alpha^*)\end{aligned} \tag{49}$$

and the resulting dynamics are

$$\frac{d\tilde{r}_c}{d\tau} = \frac{(d\hat{x}_c/d\tau)\hat{x}_c + (d\hat{y}_c/d\tau)\hat{y}_c + (d\hat{z}_c/d\tau)\hat{z}_c}{\tilde{r}_c} \tag{50}$$

$$= \frac{V_c}{\omega}\xi_c \tag{51}$$

$$\frac{d\alpha^*}{d\tau} = \frac{(d\hat{z}_c/d\tau)\sqrt{\hat{y}_c^2+\hat{x}_c^2} - \hat{z}_c(d\sqrt{\hat{y}_c^2+\hat{x}_c^2}/d\tau)}{\tilde{r}_c^2} \tag{52}$$

$$= \frac{V_c}{\omega}\left(\frac{\sin(\hat{\alpha}+a\sin(\tau))\cos(\alpha^*)}{\tilde{r}_c} - \frac{\cos(\hat{\alpha}+a\sin(\tau))\sin(\alpha^*)}{\tilde{r}_c}\cos(\hat{\theta}-\theta^*+a\cos(\tau))\right) \tag{53}$$

$$\frac{d\theta^*}{d\tau} = \frac{(d\hat{y}_c/d\tau)\hat{x}_c - \hat{y}_c(d\hat{x}_c/d\tau)}{\hat{y}_c^2+\hat{x}_c^2} \tag{54}$$

$$= \frac{V_c}{\omega}\frac{\cos(\hat{\alpha}+a\sin(\tau))}{\tilde{r}_c\cos(\alpha^*)}\sin(\hat{\theta}-\theta^*+a\cos(\tau)). \tag{55}$$

The system order can be reduced from six to five by combining $\hat{\theta}$ and θ^* into the error variable

$$\tilde{\theta} = \hat{\theta} - \theta^* \tag{56}$$

resulting in

$$\xi_c = \cos(\hat{\alpha}+a\sin(\tau))\cos(\alpha^*)\cos(\tilde{\theta}+a\cos(\tau)) + \sin(\hat{\alpha}+a\sin(\tau))\sin(\alpha^*) \tag{57}$$

and the error system

$$\frac{d\tilde{r}_c}{d\tau} = \frac{V_c}{\omega}\xi_c \tag{58}$$

$$\frac{d\alpha^*}{d\tau} = \frac{V_c}{\omega}\left(\frac{\sin(\hat{\alpha}+a\sin(\tau))\cos(\alpha^*)}{\tilde{r}_c} - \frac{\cos(\hat{\alpha}+a\sin(\tau))\sin(\alpha^*)}{\tilde{r}_c}\right)\cos(\tilde{\theta}+a\cos(\tau)) \tag{59}$$

$$\frac{d\hat{\alpha}}{d\tau} = \frac{1}{\omega}\Big(c_\alpha\xi\sin(\tau) + d_\alpha\xi^2\sin(\tau)\Big) \tag{60}$$

$$\frac{d\tilde{\theta}}{d\tau} = \frac{1}{\omega}\Big(c_\theta\xi\cos(\tau) - d_\theta\xi^2\cos(\tau)\Big) - \frac{V_c}{\omega}\frac{\cos(\hat{\alpha}+a\sin(\tau))\sin(\tilde{\theta}+a\cos(\tau))}{\tilde{r}_c\cos(\alpha^*)} \tag{61}$$

$$\frac{de}{d\tau} = \frac{h}{\omega}\xi. \tag{62}$$

As the system equations are periodic in 2π, the average error system is

$$\frac{d\tilde{r}_c^{\mathrm{ave}}}{d\tau} = \frac{V_c}{\omega}\xi_c^{\mathrm{ave}} \tag{63}$$

$$\frac{d\alpha^{*\mathrm{ave}}}{d\tau} = \frac{V_c}{\omega}\left(\frac{J_0(a)\sin(\hat{\alpha}^{\mathrm{ave}})\cos(\alpha^{*\mathrm{ave}})}{\tilde{r}_c^{\mathrm{ave}}} - \frac{J_0(\sqrt{2}a)\cos(\hat{\alpha}^{\mathrm{ave}})\sin(\alpha^{*\mathrm{ave}})\cos(\tilde{\theta}^{\mathrm{ave}})}{\tilde{r}_c^{\mathrm{ave}}}\right) \tag{64}$$

$$\frac{d\hat{\alpha}^{\mathrm{ave}}}{d\tau} = -\frac{2q_rR_1\tilde{r}_c^{\mathrm{ave}}\xi_c^{\overset{\sin}{\mathrm{ave}}}}{\omega}\left(c_\alpha - 2d_\alpha\left(q_r(\tilde{r}_c^{\mathrm{ave}^2}+R_1^2)+e^{\mathrm{ave}}\right)\right) + \frac{4d_\alpha q_r^2R_1^2\tilde{r}_c^{\mathrm{ave}^2}\xi_c^{2\,\overset{\sin}{\mathrm{ave}}}}{\omega} \tag{65}$$

$$\frac{d\tilde{\theta}^{\mathrm{ave}}}{d\tau} = -\frac{2q_rR_1\tilde{r}_c^{\mathrm{ave}}\xi_c^{\overset{\cos}{\mathrm{ave}}}}{\omega}\left(c_\theta + 2d_\theta\left(q_r(\tilde{r}_c^{\mathrm{ave}^2}+R_1^2)+e^{\mathrm{ave}}\right)\right) - \frac{4d_\theta q_r^2R_1^2\tilde{r}_c^{\mathrm{ave}^2}\xi_c^{2\,\overset{\cos}{\mathrm{ave}}}}{\omega} - J_0(\sqrt{2}a)\frac{V_c}{\omega}\frac{\cos(\hat{\alpha}^{\mathrm{ave}})\sin(\tilde{\theta}^{\mathrm{ave}})}{\tilde{r}_c^{\mathrm{ave}}\cos(\alpha^{*^{\mathrm{ave}}})} \tag{66}$$

$$\frac{de^{\mathrm{ave}}}{d\tau} = -\frac{h}{\omega}\Big(\big(q_r(\tilde{r}_c^{\mathrm{ave}^2}+R_1^2)+e\big) + 2q_rR_1\tilde{r}_c^{\mathrm{ave}}\xi_c^{\mathrm{ave}}\Big) \tag{67}$$

where[1]

$$\xi_c^{\mathrm{ave}} = J_0(\sqrt{2}a)\cos(\alpha^{*^{\mathrm{ave}}})\cos(\hat{\alpha}^{\mathrm{ave}})\cos(\tilde{\theta}^{\mathrm{ave}}) + J_0(a)\sin(\alpha^{*^{\mathrm{ave}}})\sin(\hat{\alpha}^{\mathrm{ave}}) \tag{68}$$

$$\xi_c^{\overset{\sin}{\mathrm{ave}}} = -\frac{J_1(\sqrt{2}a)}{\sqrt{2}}\cos(\alpha^{*^{\mathrm{ave}}})\sin(\hat{\alpha}^{\mathrm{ave}})\cos(\tilde{\theta}^{\mathrm{ave}}) + J_1(a)\sin(\alpha^{*^{\mathrm{ave}}})\cos(\hat{\alpha}^{\mathrm{ave}}) \tag{69}$$

$$\xi_c^{\overset{\cos}{\mathrm{ave}}} = -\frac{J_1(\sqrt{2}a)}{\sqrt{2}}\cos(\alpha^{*^{\mathrm{ave}}})\cos(\hat{\alpha}^{\mathrm{ave}})\sin(\tilde{\theta}^{\mathrm{ave}}) \tag{70}$$

$$\xi_c^{\overset{\sin}{2\,\mathrm{ave}}} = -\frac{\cos^2(\alpha^{*^{\mathrm{ave}}})}{4}\left(J_1(2a)\sin(2\hat{\alpha}^{\mathrm{ave}}) + \frac{J_1(2\sqrt{2}a)}{\sqrt{2}}\sin(2\hat{\alpha}^{\mathrm{ave}})\cos(2\tilde{\theta}^{\mathrm{ave}})\right) + J_1(2a)\frac{\sin^2(\alpha^{*^{\mathrm{ave}}})}{2}\sin(2\hat{\alpha}^{\mathrm{ave}}) + 2\frac{J_1(\sqrt{5}a)}{\sqrt{5}}\frac{\sin(2\alpha^{*^{\mathrm{ave}}})}{2}\cos(2\hat{\alpha}^{\mathrm{ave}})\cos(\tilde{\theta}^{\mathrm{ave}}) \tag{71}$$

$$\xi_c^{\overset{\cos}{2\,\mathrm{ave}}} = -\frac{\cos^2(\alpha^{*^{\mathrm{ave}}})}{4}\left(J_1(2a)\sin(2\tilde{\theta}^{\mathrm{ave}}) + \frac{J_1(2\sqrt{2}a)}{\sqrt{2}}\cos(2\hat{\alpha}^{\mathrm{ave}})\sin(2\tilde{\theta}^{\mathrm{ave}})\right) - \frac{J_1(\sqrt{5}a)}{\sqrt{5}}\frac{\sin(2\alpha^{*^{\mathrm{ave}}})}{2}\sin(2\hat{\alpha}^{\mathrm{ave}})\sin(\tilde{\theta}^{\mathrm{ave}}). \tag{72}$$

The average system (63)–(67) has equilibria defined by

$$\left[\tilde{r}_c^{\mathrm{ave}^{\mathrm{eq}_i}}, \alpha^{*^{\mathrm{ave}^{\mathrm{eq}_i}}}, \hat{\alpha}^{\mathrm{ave}^{\mathrm{eq}_i}}, \tilde{\theta}^{\mathrm{ave}^{\mathrm{eq}_i}}, e^{\mathrm{ave}^{\mathrm{eq}_i}}\right] = \left[\rho, 0, 0, (-1)^i\frac{\pi}{2}, -q_r\left(\rho^2+R_1^2\right)\right] \tag{73}$$

---

[1] Note that $\int_0^{2\pi} \mathrm{e}^{aj\sin(t)}dt = 2\pi J_0(a)$ and $\int_0^{2\pi} \mathrm{e}^{aj\,\sin(t)-jt}dt = 2\pi J_1(a)$.

for $i \in \{0,1\}$. The equilibria have the corresponding Jacobians

$$A^{\mathrm{eq}_i} = \frac{1}{\omega}\begin{bmatrix} 0 & 0 & 0 & (-1)^{i+1}m_{14} & 0 \\ 0 & -m_{22} & -m_{23} & 0 & 0 \\ 0 & m_{32} & 0 & 0 & 0 \\ (-1)^i m_{41} & 0 & 0 & -m_{44} & (-1)^i m_{45} \\ -m_{51} & 0 & 0 & (-1)^i m_{54} & -h \end{bmatrix} \tag{74}$$

where

$$m_{14} = V_c\, J_0(\sqrt{2}a) \tag{75}$$

$$m_{22} = \frac{d_\alpha\, q_r\, R_1 V_c\, J_0(\sqrt{2}a)}{c_\theta\, J_1(\sqrt{2}a)}(\sqrt{2}J_1(2a) - J_1(2\sqrt{2}a)) \tag{76}$$

$$m_{23} = 2c_\alpha\, q_r\, R_1 \rho J_1(a) \tag{77}$$

$$m_{32} = V_c\, J_0(a)\,\frac{\sqrt{\sqrt{2}}}{\rho} \tag{78}$$

$$m_{41} = m_{41a} + m_{41b} \tag{79}$$

$$m_{41a} = 4\, c_\theta\, q_r\, R_1 \frac{J_1(\sqrt{2}a)}{\sqrt{2}} \tag{80}$$

$$m_{41b} = 4\,\frac{d_\theta\, q_r\, V_c\, J_0(\sqrt{2}a)}{c_\theta} \tag{81}$$

$$m_{44} = \frac{d_\theta\, q_r\, R_1 V_c\, J_0(\sqrt{2}a)}{c_\theta\, J_1(\sqrt{2}a)}(\sqrt{2}J_1(2a) + J_1(2\sqrt{2}a)) \tag{82}$$

$$m_{45} = 4\, d_\theta\, q_r\, R_1 \rho \frac{J_1(\sqrt{2}a)}{\sqrt{2}} \tag{83}$$

$$m_{51} = 2hq_r\, \rho \tag{84}$$

$$m_{54} = 2hq_r\, R_1 \rho J_0(\sqrt{2}a). \tag{85}$$

The characteristic polynomial for these equilibria is

$$0 = ((\omega s)^2 + m_{22}\omega s + m_{32}m_{23})((\omega s)^3 + (h + m_{44})(\omega s)^2 + (hm_{44} + m_{41}m_{14} - m_{54}m_{45})\omega s + hm_{14}m_{41a}).$$

The second-order polynomial has roots with negative real parts as both m_{22} and $m_{32}m_{23}$ are positive. The third-order polynomial has roots with negative real parts as, according to the assumptions in Theorem 1, all the coefficients are positive and the product of the s^2 and s^1 coefficients is greater than the s^0 coefficient. Therefore, the Jacobians (74) are Hurwitz given the assumptions in Theorem 1. As such, the equilibria (74) are exponentially stable. By applying [22, Th. 10.4] to this result, we conclude that the error system (63)–(67) has distinct, exponentially stable periodic solutions within $O(1/\omega)$ of the equilibria (73) defined by

$$\tilde{r}_c^{\mathrm{attr}_i}(\tau) = \rho + \tilde{r}_c^{2\pi^{\mathrm{eq}_i}}(\tau) \tag{86}$$

$$\alpha^{*\mathrm{attr}_i}(\tau) = \alpha^{*2\pi^{\mathrm{eq}_i}}(\tau) \tag{87}$$

$$\hat{\alpha}^{\mathrm{attr}_i}(\tau) = \hat{\alpha}^{2\pi^{\mathrm{eq}_i}}(\tau) \tag{88}$$

$$\tilde{\theta}^{\mathrm{attr}_i}(\tau) = (-1)^i \frac{\pi}{2} + \tilde{\theta}^{2\pi^{\mathrm{eq}_i}}(\tau) \tag{89}$$

$$e^{\mathrm{attr}_i}(\tau) = -q_r\left(\rho^2 + R_1^2\right) + e^{2\pi^{\mathrm{eq}_i}}(\tau) \tag{90}$$

where $\tilde{r}_c^{2\pi^{\mathrm{eq}_i}}(\tau)$, $\alpha^{*2\pi^{\mathrm{eq}_i}}(\tau)$, $\hat{\alpha}^{2\pi^{\mathrm{eq}_i}}(\tau)$, $\tilde{\theta}^{2\pi^{\mathrm{eq}_i}}(\tau)$, and $e^{2\pi^{\mathrm{eq}_i}}(\tau)$ are periodic with period 2π and are $O(1/\omega)$. This indicates that the angle α^* remains within $O(1/\omega)$ of $m\pi$ and the distance between the vehicle center r_c and the source r^* converges to within $O(1/\omega)$ of the value $\rho = \sqrt{V_c J_0(\sqrt{2}a)/\sqrt{2}c_\theta q_r R_1 J_1(\sqrt{2}a)}$. The set $\mathcal{T}_{O(1/\omega)}$ defined in Theorem 1 can be derived from this set. As the attractive solution of e is a periodic function within $O(1/\omega)$ of $-q_r R_1^2 - [V_c J_0(\sqrt{2}a)/\sqrt{2}c_\theta R_1 J_1(\sqrt{2}a)]$, the sensor reading $J(t)$ converges to a periodic function within $O(1/\omega)$ of $f^* - q_r R_1^2 - [V_c J_0(\sqrt{2}a)/\sqrt{2}c_\theta q_r R_1 J_1(\sqrt{2}a)]$. To prove the last part of the theorem, we first note that while the error system (63)–(67) has five states, the (shifted) physical system from which the error system was derived has six, the three state vector $\hat{r}_c$, the two angles $\hat{\alpha}$ and $\hat{\theta}$, and e. To study the attractive solutions of $\hat{r}_c$ and thus x_c, y_c, z_c, we start by first determining the θ^* part of the attractor solution from $d\theta^*/d\tau = (V_c/\omega)[\cos(\hat{\alpha} + a\sin(\tau))\sin(\tilde{\theta} + a\cos(\tau))/\tilde{r}_c\cos(\alpha^*)]$. We substitute the attractor solution (86)–(90) of the error solution and find

$$\theta^{*\mathrm{attr}_i}(t) = (-1)^i\left(\frac{V_c}{\rho}\left(1 + \lambda_\mu^{\mathrm{eq}_i}\right)t + \frac{V_c}{\rho}\beta_0^{\frac{2\pi}{\omega}^{\mathrm{eq}_i}}(t) + \gamma^{\mathrm{eq}_i}\right)$$

where γ^{eq_i} is a constant, $\lambda_\mu^{\mathrm{eq}_i} = \frac{1}{2\pi}\int_0^{2\pi}\lambda^{2\pi^{\mathrm{eq}_i}}(\tau)d\tau$ is the mean of[2]

$$\begin{aligned}\lambda^{2\pi^{\mathrm{eq}_i}}(\tau) = &-2\sin^2\left(\frac{\tilde{\theta}^{2\pi^{\mathrm{eq}_i}}(\tau) + a\cos(\tau)}{2}\right) \\ &- 2\sin^2\left(\frac{\hat{\alpha}^{2\pi^{\mathrm{eq}_i}}(\tau) + a\,\sin(\tau)}{2}\right) \\ &\times\cos(\tilde{\theta}^{2\pi^{\mathrm{eq}_i}}(\tau) + a\cos(\tau)) \\ &+ \frac{\cos\left(\hat{\alpha}^{2\pi^{\mathrm{eq}_i}}(\tau) + a\sin(\tau)\right)}{1 - 2\sin^2\left(\alpha^{*2\pi^{\mathrm{eq}_i}}(\tau)/2\right)} \\ &\times\cos(\tilde{\theta}^{2\pi^{\mathrm{eq}_i}}(\tau) + a\cos(\tau)) \\ &\times\left(2\sin^2(\alpha^{*2\pi^{\mathrm{eq}_i}}(\tau)/2) - \frac{\tilde{r}_c^{2\pi^{\mathrm{eq}_i}}(\tau)}{\rho + \tilde{r}_c^{2\pi^{\mathrm{eq}_i}}(\tau)}\right)\end{aligned}$$

and it is $O(a^2) + O(1/\omega)$. The quantity $\lambda_0^{(2\pi/\omega)^{\mathrm{eq}_i}}(t) = \lambda^{(2\pi/\omega)^{\mathrm{eq}_i}}(t) - \lambda_\mu^{\mathrm{eq}_i}$ is the zero-mean part of $\lambda^{(2\pi/\omega)^{\mathrm{eq}_i}}(t)$, and $\beta_0^{(2\pi/\omega)^{\mathrm{eq}_i}}(t)$ is the integral of $\lambda_0^{(2\pi/\omega)^{\mathrm{eq}_i}}(t)$, is periodic with frequency ω, and is zero mean. Both $\lambda_0^{(2\pi/\omega)^{\mathrm{eq}_i}}(t)$ and $\beta_0^{(2\pi/\omega)^{\mathrm{eq}_i}}(t)$ are $O(a^2) + O(1/\omega)$. By splitting $\tilde{r}_c^{(2\pi/\omega)^{\mathrm{eq}_i}}(\tau)$ and $\alpha^{*(2\pi/\omega)^{\mathrm{eq}_i}}(\tau)$ into $\tilde{r}_\mu^{\mathrm{eq}_i} + \tilde{r}_{c_0}^{(2\pi/\omega)^{\mathrm{eq}_i}}(t)$ and $\alpha_\mu^{*\mathrm{eq}_i} + \alpha_0^{*(2\pi/\omega)^{\mathrm{eq}_i}}(t)$, where $\tilde{r}_\mu^{\mathrm{eq}_i} = (1/2\pi)\int_0^{2\pi}\tilde{r}_c^{2\pi^{\mathrm{eq}_i}}(\tau)d\tau$ is $O(1/\omega)$ and the mean of $\tilde{r}_c^{(2\pi/\omega)^{\mathrm{eq}_i}}(t)$, $\alpha_\mu^{*\mathrm{eq}_i} = (1/2\pi)\int_0^{2\pi}\alpha^{*2\pi^{\mathrm{eq}_i}}(\tau)d\tau$ is $O(1/\omega)$ and the mean of

---

[2] To avoid confusion between functions with period 2π, $f^{2\pi}(\tau)$, and functions with period $2\pi/\omega$, $f^{(2\pi/\omega)}(t)$, recall the transformation $\tau = \omega t$.

$\alpha^{*(2\pi/\omega)^{\mathrm{eq}_i}}(t)$ and both $\tilde{r}_{c_0}^{(2\pi/\omega)^{\mathrm{eq}_i}}(t) = \tilde{r}_c^{(2\pi/\omega)^{\mathrm{eq}_i}}(t) - \tilde{r}_\mu^{\mathrm{eq}_i}$ and $\alpha_0^{*(2\pi/\omega)^{\mathrm{eq}_i}}(t) = \alpha^{*(2\pi/\omega)^{\mathrm{eq}_i}}(t) - \alpha_\mu^{*\mathrm{eq}_i}$ are periodic, zero mean, and $O(1/\omega)$, we find (13)–(15). ■

REFERENCES

[1] J. Cochran and M. Krstic, "Nonholonomic source seeking with tuning of angular velocity," *IEEE Trans. Autom. Control*, to be published.

[2] C. Zhang, D. Arnold, N. Ghods, A. Siranosian, and M. Krstic, "Source seeking with nonholonomic unicycle without position measurement and with tuning of forward velocity," *Syst. Control Lett.*, vol. 56, pp. 245–252, 2007.

[3] J. Cochran and M. Krstic, "Source seeking with a nonholonomic unicycle without position measurements and with tuning of angular velocity—Part I: Stability analysis," in *Proc. 2007 Conf. Decision Control*, pp. 6009–6016.

[4] J. Cochran, A. Siranosian, N. Ghods, and M. Krstic, "Source seeking with a nonholonomic unicycle without position measurements and with tuning of angular velocity—Part II: Applications," in *Proc. 2007 Conf. Decision Control*, pp. 1951–1956.

[5] B. Porat and A. Neohorai, "Localizing vapor-emitting sources by moving sensors," *IEEE Trans. Signal Process.*, vol. 44, no. 4, pp. 1018–1021, Apr. 1996.

[6] P. Reddy, E. Justh, and P. Krishnaprasad, "Motion camouflage in three dimensions," in *Proc. 45th IEEE Conf. Decision Control*, 2006, pp. 3327–3332.

[7] P. Ogren, E. Fiorelli, and N. Leonard, "Cooperative control of mobile sensor networks: Adaptive gradient climbing in a distributed environment," *IEEE Trans. Autom. Control*, vol. 29, no. 8, pp. 1292–1302, Aug. 2004.

[8] D. J. Klein, C. Matlack, and K. A. Morgansen, "Cooperative target tracking using oscillator models in three dimensions," in *Proc. 2007 Amer. Control Conf.*, New York, pp. 2569–2575.

[9] K. Peterson and A. Stefanopoulou, "Extremum seeking control for soft landing of and electromechanical valve actuator," *Automatica*, vol. 29, pp. 1063–1069, 2004.

[10] Y. Ou, C. Xu, E. Schuster, T. Luce, J. R. Ferron, and M. Walker, "Extremum-seeking finite-time optimal control of plasma current profile at the diii-d tokamak," in *Proc. 2007 Amer. Control Conf.*, pp. 4015–4020.

[11] C. Centioli, F. Iannone, G. Mazza, M. Panella, L. Pangione, S. Podda, A. Tuccillo, V. Vitale, and L. Zaccarian, "Extremum seeking applied to the plasma control system of the Frascati Tokamak upgrade," in *Proc. 44th IEEE Conf. Decision Control, Eur. Control Conf.*, 2005, pp. 8227–8232.

[12] Y. Tan, D. Nesic, and I. M. Y. Mareels, "On non-local stability properties of extremum seeking controllers," *Automatica*, vol. 42, pp. 889–903, 2006.

[13] R. King, R. Becker, G. Feuerbach, L. Henning, R. Petz, W. Nitsche, O. Lemke, and W. Neise, "Adaptive flow control using slope seeking," in *Proc. 14th IEEE Mediterranean Conf. Control Autom.*, 2006, pp. 1–6.

[14] R. Becker, R. King, R. Petz, and W. Nitsche, "Adaptive closed-loop separation control on a high-lift configuration using extremum seeking," presented at the 3rd AIAA Flow Control Conf., San Francisco, CA, 2006.

[15] M. Tanelli, A. Astolfi, and S. Savaresi, "Non-local extremum seeking control for active braking control systems," in *Proc. Conf. Control Appl.*, Munich, Germany, 2006, pp. 891–896.

[16] Y. Li, A. Rotea, G. T.-C. Chiu, L. Mongeau, and I.-S. Paek, "Extremum seeking control of a tunable thermoacoustic cooler," *IEEE Trans. Control Syst. Technol.*, vol. 13, no. 4, pp. 527–536, Jul. 2005.

[17] X. Zhang, D. Dawson, W. Dixon, and B. Xian, "Extremum seeking nonlinear controllers for a human exercise machine," in *Proc. 2004 IEEE Conf. Decision Control*, pp. 233–240.

[18] D. Baronov and J. Baillieul, "Reactive exploration through following isolines in a potential field," in *Proc. 2007 Amer. Control Conf.*, New York, 2007, pp. 2141–2146.

[19] K. Ariyur and M. Krstic, *Real-Time Optimization by Extremum-Seeking Control*. Hoboken, NJ: Wiley, 2003.

[20] H.-H. Wang, S. Yeung, and M. Krstic, "Experimental application of extremum seeking on an axial-flow compressor," *IEEE Trans. Control Syst. Technol.*, vol. 8, no. 2, pp. 300–309, Mar. 1999.

[21] S. Kalantar and U. Zimmer, "Control of open contour formations of autonomous underwater vehicles," *Int. J. Adv. Robot. Syst.*, vol. 2, no. 4, pp. 309–316, Dec. 2005.

[22] H. Khalil, *Nonlinear Systems*, 3rd ed. Upper Saddle River, NJ: Prentice-Hall, 2002.

Jennie Cochran (S'06–M'09) received the Undergraduate and Master's degrees from the Department of Computer Science and Engineering, Massachusetts Institute of Technology, Boston, and the Ph. D. degree in dynamic systems and control from the University of California, San Diego, in 2008.

She is currently a Scientific Analyst for ScienceOps, Bothell, WA. Dr. Cochran was the recipient of the National Defense Science and Engineering Graduate Student Fellowship.

Antranik Siranosian (S'07) received the B.S. degree in mechanical engineering from California State Polytechnic University, Pomona, in 2003, and the M.S. and Ph.D. degrees in dynamic systems and control from the University of California (UC), San Diego, in 2005 and 2008, respectively.

He is currently with the Department of Mechanical and Aerospace Engineering, UC. His current research interests include nonlinear and adaptive control for shake tables and autonomous vehicles, as well as trajectory generation and tracking for finite- and infinite-dimensional systems.

Nima Ghods (S'09) received the B.S. degree in mechanical engineering in 2006 and the M.E. degree in aerospace engineering in 2007 from the University of California (UC), San Diego, where he is currently working toward the Ph.D. degree in dynamic systems and control.

His current research interests include extremum seeking control theory and application on mobile vehicles and cooperative control of multiple autonomous agents.

Miroslav Krstic (S'92–M'95–SM'99–F'02) received the B.S. degree from the University of Belgrade, Belgrade, Yugoslavia, and the M.S. and Ph.D. degrees from the University of California, Santa Barbara, in 1989, 1992, and 1994, respectively, all in electrical engineering.

He is the Sorenson Distinguished Professor and the Founding Director of the Cymer Center for Control Systems and Dynamics, University of California, San Diego (UCSD). He has authored or coauthored the books *Nonlinear and Adaptive Control Design* (1995), *Stabilization of Nonlinear Uncertain Systems* (1998), *Flow Control by Feedback* (2002), *Real-time Optimization by Extremum Seeking Control* (2003), *Control of Turbulent and Magnetohydrodynamic Channel Flows* (2007), and *Boundary Control of PDEs: A Course on Backstepping Designs* (2008).

Prof. Krstic was the recipient of the Axelby, Schuck, the National Science Foundation (NSF) Career, the Office of Naval Research (ONR) YI, and Presidential Early Career Award for Scientists and Engineers (PECASE) Awards, the UCSD Research Award. He is a Fellow of the International Federation of Automatic Control (IFAC), and has held the Springer Distinguished Professorship at the UC, Berkeley. His editorial service includes the IEEE TRANSACTIONS ON AUTOMATIC CONTROL (IEEE TAC), the *Automatica*, the *Society of Composers and Lyricists* (SCL), and the *International Journal of Adaptive Control and Signal Processing* (IJACSP). He was the Vice President (VP) Technical Activities with the Control Systems Society (CSS) and the Chair of the IEEE Fellow Committee.